Polarized spectral properties and 2.3 μm laser performance of the Tm:YVO 4 crystal

Xiaoxu Yu, Kirill Eremeev, Zhongben Pan, Pavel Loiko, Hongwei Chu, Han Pan, Alain Braud, Patrice Camy, Dechun Li

▶ **To cite this version:**

Xiaoxu Yu, Kirill Eremeev, Zhongben Pan, Pavel Loiko, Hongwei Chu, et al.. Polarized spectral properties and 2.3 μm laser performance of the Tm:YVO 4 crystal. Optics Express, 2024, 32 (10), pp.18055. ⟨10.1364/OE.524153⟩. ⟨hal-04776147⟩

HAL Id: hal-04776147

https://hal.science/hal-04776147v1

Submitted on 11 Nov 2024

HAL is a multi-disciplinary open access archive for the deposit and dissemination of scientific research documents, whether they are published or not. The documents may come from teaching and research institutions in France or abroad, or from public or private research centers.

L'archive ouverte pluridisciplinaire **HAL**, est destinée au dépôt et à la diffusion de documents scientifiques de niveau recherche, publiés ou non, émanant des établissements d'enseignement et de recherche français ou étrangers, des laboratoires publics ou privés.

HAL Authorization

Polarized spectral properties and 2.3 μm laser performance of the Tm:YVO_4 crystal

Xiaoxu Yu,[1] Kirill Eremeev,[2] Zhongben Pan,[1,*] Pavel Loiko,[2] Hongwei Chu,[1] Han Pan,[1] Alain Braud,[2] Patrice Camy,[2] and Dechun Li[1,*]

[1]School of Information Science and Engineering, and Key Laboratory of Laser and Infrared System of Ministry of Education, Shandong University, Qingdao 266237, China
[2]Centre de Recherche sur les Ions, les Matériaux et la Photonique (CIMAP), UMR 6252 CEA-CNRS-ENSICAEN, Université de Caen Normandie, 6 Boulevard Maréchal Juin, 14050 Caen Cedex 4, France
**zhongbenpan@sdu.edu.cn; dechun@sdu.edu.cn*

Abstract: The polarized spectral properties and ~2.3 μm high-power continuous-wave laser operation of Tm^{3+}-doped yttrium orthovanadate crystal (Tm:YVO_4) are reported. For the $^3H_4 \rightarrow {}^3H_5$ transition, the stimulated-emission cross-section σ_{SE} is 1.01×10^{-20} cm^2 at 2276 nm corresponding to a large emission bandwidth of 52 nm (for π-polarization). Pumped by a 794 nm laser diode, the 1.5 at.% Tm:YVO_4 laser delivered 5.52 W at 2.29 μm with a slope efficiency of 19.9%, a laser threshold of 8.70 W, and a linear laser polarization (π). The Tm laser operated on the cascade scheme (on the $^3H_4 \rightarrow {}^3H_5$ and $^3F_4 \rightarrow {}^3H_6$ transitions) which was mainly responsible for the observed high laser slope efficiency. We also report on the first passively Q-switched Tm:YVO_4 laser at 2.3 μm by employing porous nano-grained cuprous selenide (PNG-Cu_2Se) as a saturable absorber. The shortest pulse duration and the highest single pulse energy amounted to 706 ns and 3.65 μJ, respectively, corresponding to a pulse repetition rate of 62.8 kHz.

© 2024 Optical Society of America under the terms of the OSA Open Access Publishing Agreement

1. Introduction

Nowadays, short-wave infrared (SWIR) laser sources are under rapid development due to their potential for important scientific and technological applications. This spectral range can be accessed by using the direct generation of coherent radiation from solid-state gain media doped with transition-metal (Cr^{2+} [1] and Fe^{2+} [2]) or rare-earth ions (Dy^{3+} [3], Ho^{3+} [4], Er^{3+} [5], and Tm^{3+} [6]). In recent years, laser sources emitting at 2.2-2.4 μm were a great deal of interest due to their promising applications in non-invasive glucose blood measurement [7], atmospheric environment monitoring [8], pumping of optical parametric oscillators [9], and fiber gas photonics. The $^3H_4 \rightarrow {}^3H_5$ transition of thulium (Tm^{3+}) ions falls right into this spectral range. The generation of laser radiation at 2.3 μm from diode-pumped Tm lasers is a relatively simple and cost-efficient method.

The rare-earth orthovanadate ($REVO_4$) crystals feature a high thermal conductivity [10] and weak thermal expansion, making them well-suited for high-power lasers [11, 12]. Tm^{3+} ions in $REVO_4$ possess a broad and intense absorption band (the $^3H_6 \rightarrow {}^3H_4$ transition) and can be efficiently pumped by high-power spatially multimode fiber-coupled AlGaAs laser diodes (LDs) emitting around 0.8 μm [11, 13, 14]. Excellent performance of these crystals for ~2.3 μm high-power solid-state lasers has been demonstrated in our previous studies [15-18]. Although some other Tm^{3+}-doped crystals, such as Tm:$Y_3Al_5O_{12}$ [19, 20], Tm:$YAlO_3$ [19, 21], and Tm:$LiYF_4$ [19, 22], have also been employed in continuous wave (CW) ~2.3 μm diode-pumped lasers, their respective output powers were limited (<3 W). The schemes for optimizing the output performance of diode-pumped 2.3-μm Tm lasers have been barely studied.

Cascade lasing is a phenomenon in which two successive laser transitions could facilitate each other and this strategy was widely used in lasers based on rare-earth ions with a metastable lower-lying excited state, such as Tm^{3+} [23], Er^{3+} [24], Ho^{3+} [25, 26], and Dy^{3+} [27]. For Tm^{3+},

it implies the simultaneous operation on the $^3H_4 \rightarrow {}^3H_5$ and $^3F_4 \rightarrow {}^3H_6$ laser transitions. Recently, the cascade laser strategy has been proven to be a promising approach to improve the output performance of 2.3-μm Tm lasers [28]. However, since the energy-transfer upconversion (ETU, $^3F_4 + {}^3F_4 \rightarrow {}^3H_6 + {}^3H_4$) process, which is favorable for the $^3H_4 \rightarrow {}^3H_5$ Tm^{3+} transition, can be strongly reduced when the cascade laser operation is allowed, the latter effect does not always improve the 2.3 μm laser performance [29].

Due to the large quantum defect and easily quenched upper laser level ($^3H_4$) lifetime by both the multiphonon non-radiative relaxation and cross-relaxation (CR, $^3H_4 + {}^3H_6 \rightarrow {}^3F_4 + {}^3F_4$), severe thermal effects are expected in high-power diode-pumped 2.3 μm Tm lasers. Pumping into the sidebands of the absorption peak is an efficient way to alleviate thermal issues. In this pumping scheme, the uniformity of longitudinal temperature distribution is improved by reducing the front-end absorption. The use of long crystals enables good heat removal and reduces thermal loading. This scheme has been widely exploited in 1 μm and 2 μm lasers [30, 31]. However, to the best of our knowledge, there are no reports on the improvement of the performance of 2.3-μm Tm lasers via this pumping scheme.

So far, the highest 2.3 μm CW output power was obtained using a Tm^{3+}-doped gadolinium vanadate crystal, Tm:$GdVO_4$ [18]. From the point of view of crystal growth, its lutetium and yttrium counterparts ($LuVO_4$ and YVO_4, respectively) are more suitable for doping with Tm^{3+} due to the closer ionic radii of the dopant ions (R_{Tm} = 0.994 Å), and the host-forming cations, Lu^{3+} and Y^{3+} (R_{Lu} = 0.977 Å and R_Y = 1.019 Å) compared with that of Gd^{3+} (R_{Gd} = 1.053 Å, for VIII-fold oxygen coordination). Due to the inferior thermo-mechanical properties (compared to other orthovanadates), the Tm:$LuVO_4$ crystals fracture at high pump levels, resulting in the maximum CW laser output power at 2.3 μm below 1 W [32].

In the present work, we report on the high-power continuous-wave laser operation of the Tm:YVO_4 crystal at 2.3 μm. The cascade laser scheme and the weaker absorption pumping strategy were used to boost the laser performance. The first passively Q-switched 2.3-μm Tm:YVO_4 laser is also reported.

2. Polarized spectral properties

The absorption spectra were measured using a spectrophotometer (Lambda 1050, Perkin Elmer). The luminescence of Tm^{3+} ions was excited using a Ti:Sapphire laser, collected using a set of CaF_2 lenses coupling the light into a ZrF_4 fiber, and detected using an optical spectrum analyzer (Yokogawa AQ6376). It was purged with N_2 gas to eliminate the effect of the structured water vapor absorption. A Glan-Taylor prism was used for polarized measurements. The luminescence decay curves were measured using an ns optical parametric oscillator (OPO, Horizon, Continuum), a 1/4 m monochromator (Oriel 77200), a fast InGaAs detector, and an 8 GHz digital oscilloscope (DSA70804B, Tektronix).

Figure 1 (b) shows the polarized absorption cross-sections, σ_{abs}, spectra for the $^3H_6 \rightarrow {}^3H_4$ pump transition of Tm^{3+} ions in the YVO_4 crystal. The peak σ_{abs} values amount to 3.22×10^{-20} cm^2 at 798.5 nm and 2.52×10^{-20} cm^2 at 796.9 nm, for π and σ polarizations, respectively. For the former polarization, the absorption bandwidth (full width at half maximum, FWHM) is 12 nm. For σ polarized light, it is even broader, about 20 nm.

The stimulated-emission (SE) cross-sections, σ_{SE}, for transitions of Tm^{3+} ions falling into the SWIR spectral range ($^3F_4 \rightarrow {}^3H_6$ and $^3H_4 \rightarrow {}^3H_5$), were calculated using the Füchtbauer-Ladenburg formula [36] from the measured luminescence spectra:

$$\sigma_{SE}^{i}(\lambda) = \frac{\lambda^5}{8\pi < n >^2 \tau_{rad} c} \cdot \frac{W_i(\lambda)\beta_{JJ'}}{1/3 \sum_{j=2\sigma,\pi} \int \lambda W_j(\lambda) d\lambda} \quad (1)$$

where λ is the emission wavelength, $< n >$ is the average refractive index at the mean emission wavelength of the considered transition, c is the light speed, τ_{rad} is the radiative lifetime of the emitting multiplet ($^3H_4$ or $^3F_4$), $W_i(\lambda)$ is the luminescence spectrum corrected for the apparatus response of the set-up and the structured water vapor absorption in the air, i denotes the light polarization (π and σ), and $\beta_{JJ'}$ is the luminescence branching ratio for the particular transition.

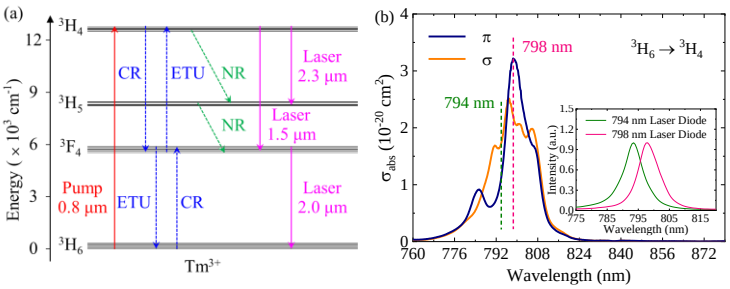

Fig. 1. (a) A partial energy-level scheme of Tm^{3+} in the YVO_4 crystal: *red* and *pink* arrows, pump absorption and laser transitions, respectively; *green* arrows, non-radiative (NR) relaxation; *blue* arrows, cross-relaxation (CR) and energy-transfer upconversion (ETU) processes; (b) absorption cross-sections, σ_{abs}, for the $^3H_6 \rightarrow {}^3H_4$ Tm^{3+} transition for π and σ polarizations, *pink* line - peak pumping, *green* line - sideband pumping; *inset*: typical emission spectra of the two used laser diodes.

The σ_{SE} spectra for the $^3F_4 \rightarrow {}^3H_6$ and $^3H_4 \rightarrow {}^3H_5$ Tm^{3+} transitions are shown in Fig. 2 (a). Here, we used the following spectroscopic data: τ_{rad} ($^3F_4$) = 1.21 ms, τ_{rad} ($^3H_4$) = 224 μs, and $\beta_{JJ'}$ ($^3H_4 \rightarrow {}^3H_5$) = 4.0% obtained using the Judd-Ofelt theory [37]. For the $^3F_4 \rightarrow {}^3H_6$ transition, the maximum σ_{SE} reaches 2.35×10^{-20} cm^2 at 1812.5 nm for π-polarization and 2.04×10^{-20} cm^2 at 1807.7 nm for σ-polarized light. In the long-wave spectral range where laser operation is expected due to the reabsorption losses (quasi-three-level laser scheme), σ_{SE} is 1.69×10^{-20} cm^2 at 1850.9 nm for σ-polarization.

For the $^3H_4 \rightarrow {}^3H_5$ transition, the emission spectra are smooth and broad extending from 2.14 to 2.4 μm. For σ-polarized light, the maximum σ_{SE} amounts to 1.07×10^{-20} cm^2 at 2213 nm and the emission bandwidth (FWHM) reaches 120 nm. This emission bandwidth is close to that of the structurally disordered Tm:$CaGdAlO_4$ crystal with a strong inhomogeneous spectral line broadening (128 nm for σ-polarization, 226 nm for π-polarization [28]) and is the broadest one among other commonly used Tm^{3+}-doped oxide and fluoride ordered laser crystals, Table 1. This indicates the capability of Tm:YVO_4 to support ultrashort pulse generation (hundreds of fs) in mode-locked lasers, as well as broad wavelength tunability. For π-polarization, the most intense emission peak is found at 2276 nm with σ_{SE} of 1.01×10^{-20} cm^2 (emission bandwidth: 52 nm). Two weaker emission peaks are found at 2172 nm and 2365 nm and the corresponding σ_{SE} is 0.77×10^{-20} cm^2 (FWHM = 75 nm) and 0.82×10^{-20} cm^2 (FWHM = 38 nm), respectively. Figure 2 (b) shows the luminescence decay curves from the $^3F_4$ and $^3H_4$ states of Tm^{3+} ions measured under resonant excitation. For the doping level of 2.5 at.% Tm, the luminescence lifetimes τ_{lum} are 1.16 ms and 36 μs, respectively.

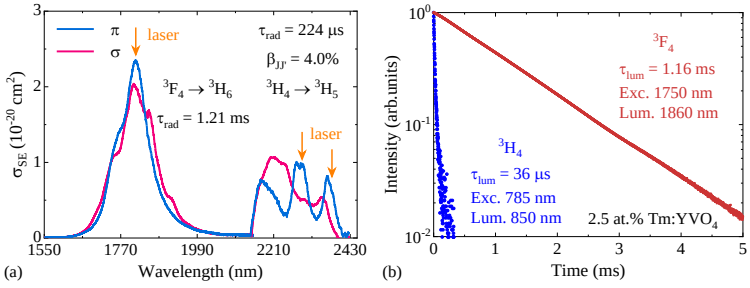

Fig. 2. Short-wave infrared emission properties of Tm^{3+} ions in YVO_4: (a) stimulated-emission cross-sections, σ_{SE}, for the $^3F_4 \rightarrow {}^3H_6$ and $^3H_4 \rightarrow {}^3H_5$ transitions for π and σ polarizations; (b)

luminescence decay curves from the $^3F_4$ and $^3H_4$ Tm^{3+} states measured under resonant excitation.

Table 1. Absorption and Stimulated-Emission Properties of Tm^{3+} Ions in Crystals Employed in 2.3-μm Lasers[a]

Gain medium	Absorption ($^3H_6 \rightarrow {}^3H_4$)			Stimulated emission ($^3H_4 \rightarrow {}^3H_5$)				Ref.
	σ_{abs} (10^{-20} cm^2)	Polariz.	FWHM (nm)	σ_{SE} (10^{-20} cm^2)	λ_{em} (nm)	Polariz.	FWHM (nm)	
Oxides (aluminates)								
Tm:$YAlO_3$	1.19	$\boldsymbol{E} \parallel \boldsymbol{b}$	4	0.78	2278	$\boldsymbol{E} \parallel \boldsymbol{b}$	12	[21]
Tm:$Y_3Al_5O_{12}$	0.65	-	3	0.35	2324	-	37	[20, 35]
Tm:$CaGdAlO_4$	1.59	π	16	1.14	2324	σ	128	[28]
Oxides (vanadates)								
Tm:$GdVO_4$	3.29	π	7	2.97	2280	π	42	[18]
Tm:$LuVO_4$	6.32	π	6	2.48	2363	π	28	[32]
Tm:YVO_4	3.22	π	**12**	1.01	2276	π	**52**	This work
	2.52	σ	**20**	1.07	2213	σ	**120**	
Fluorides								
Tm:$LiYF_4$	0.64	π	-	0.57	2305	π	25.8	[22, 33]
Tm:KY_3F_{10}	0.66	-	3.8	0.34	2345	-	53.8	[34]

[a] σ_{abs} - peak absorption cross-section; σ_{SE} - peak stimulated-emission cross-section; λ_{abs} and λ_{em} - wavelengths corresponding to the absorption and emission peaks; Polariz. - light polarization; FWHM - bandwidth of the absorption and emission peak (full width at half maximum).

3. Laser operation

3.1 Laser set-up

Two Tm:YVO_4 crystals grown by the conventional Czochralski method with different Tm^{3+} doping levels of 1.5 at.% and 2.5 at.% were employed as gain media. The actual Tm^{3+} ion densities N_{Tm} were 1.87×10^{20} cm^{-3} and 3.12×10^{20} cm^{-3}, respectively. Rectangular laser elements with an aperture of 3×3 mm^2 and a thickness of 10 mm were oriented for light propagation along the ***a*** crystallographic axis (***a***-cut). Both their input and output faces were polished to laser-grade quality and antireflection (AR) coated for the pump, 790 ± 10 nm (reflectance (R) < 0.5%), and laser radiation, 1850-2360 nm (R < 1%). The schematic of the diode-pumped Tm:YVO_4 laser is shown in Fig. 3 (a). Two fiber-coupled spatially multimode AlGaAs laser diodes (fiber core diameter: 200 μm, numerical aperture (N.A.): 0.22) with the center emission wavelengths of 798 nm and 794 nm were used to perform the strongest absorption pumping and weaker absorption pumping scheme, respectively. Their spectra are shown in Fig. 1 (c) (*inset*). Although the pump wavelength of 794 nm is very close to that of 798 nm, their corresponding absorption cross-sections are very different, 3.22×10^{-20} cm^2 at 798.5 nm and 1.12×10^{-20} cm^2 at 794 nm (π-polarization). The pump beam was reimaged into the laser crystal by a pair of plano-convex lenses (focal length: f = 50 mm) with an imaging ratio of 1:1. A simple compact plano-plano laser cavity with a geometrical length of 13 mm was employed. It consisted of a flat pump mirror (PM) coated for high transmission at 0.79 μm and high reflection at 1.8-2.4 μm and a set of plane output couplers (OCs) providing a transmission T_{OC} ranging from 0.5% to 10% at 2.2-2.4 μm. All the OCs additionally provided a high transmission of ~90% around 2 μm. The laser crystal was placed close to the PM and wrapped with indium foil and then mounted inside a water-cooled copper block with the temperature set at 12 °C.

The residual pump beam was filtered out using a long-pass filter (F_1, FELH900, Thorlabs) with high transmission at above 1 μm (about 85% at 2.3 μm). Another long-pass filter (F_2) transmitting ~90% at 2.3 μm and almost zero at 2 μm was used to separate the 2.3 μm power contribution. The actual filter transmission at the laser wavelength was considered to determine the actual output power. The laser output power and emission spectra were measured with an optical power meter (S425C+PM400, Thorlabs) and an optical spectrum analyzer (APE GmbH, Germany), respectively. The intensity profile of the laser beam was captured using a pyroelectric camera (WinCamD-IR-BB, Serial # 70381). The pulsed output from the Q-

switched laser was detected by a photodetector (Vigo System) and observed by an oscilloscope (DPO 7104C, Tektronix Inc.).

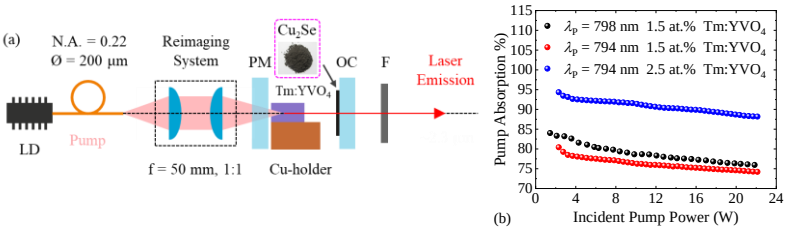

Fig. 3. (a) Schematic of the diode-pumped Tm:YVO_4 laser: PM - pump mirror; OC - output coupler; F - long-pass filter; (b) single-pass pump absorption efficiency measured under non-lasing conditions as a function of the incident pump power at 794 nm and 798 nm.

3.2 Continuous-wave laser operation

The absorbed pump power (P_{abs}) was calculated for single-pass pumping since all the OCs featured high transmission at 0.79 μm. The pump absorption efficiencies under non-lasing conditions $\eta_{abs,NL} = P_{abs} / P_{inc}$ (P_{inc} - incident pump power) for the two studied Tm:YVO_4 crystals pumped by 794-nm and 798-nm laser diodes were determined in a pump-transmission experiment. As shown in Fig. 3 (b), the pumping scheme with the strongest absorption provides only a slight improvement of the pump absorption efficiency ranging from 84% to 76% as compared to the weaker absorption pumping scheme, for which this parameter lines in the range of 80.4% to 74.2%, for 1.5 at.% Tm^{3+} doping level. A noticeable absorption saturation was observed as the incident pump power increased due to the ground-state ($^3H_6$) bleaching and the slight temperature shift of the diode emission wavelength.

The laser performance of the 2.5 at.% Tm:YVO_4 crystal was first studied due to its higher pump absorption efficiency in the range of 94.3%-88.2% (pumping at 794 nm). However, the maximum extracted CW laser output power was only 406 mW at 2.29 μm with a high laser threshold of P_{inc} = 6.99 W (for 0.5% OC) and a slope efficiency of 8.5%, as shown in Fig. 4, which could be caused by the quenched upper laser level ($^3H_4$) lifetime through the severe CR process. For the Tm^{3+} doping level of 2.5 at.%, the luminescence lifetime of the $^3H_4$ state is about 36 μs.

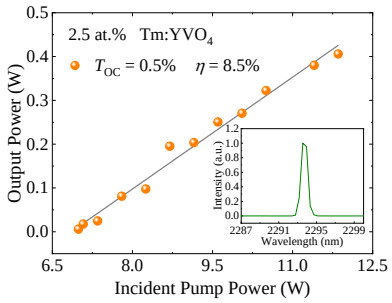

Fig. 4. Diode-pumped 2.5 at.% Tm:YVO_4 laser: input-output dependence and the laser emission spectrum (*inset*) for 0.5% OC.

For the 1.5 at.% Tm^{3+} doping level, the input-output dependences of the diode-pumped Tm:YVO_4 lasers for pumping at the strongest absorption (at 798 nm) and weaker absorption (at 794 nm) are compared in Fig. 5. The full details about the laser parameters not mentioned

in the following text can be found in Table 2. This optimum Tm^{3+} doping level of 1.5 at.% was selected due to the two following reasons. First, for a high Tm^{3+} doping level, the fluorescence lifetime of the $^3H_4$ manifold will be significantly quenched by cross-relaxation among adjacent Tm^{3+} ions, which is favoring the unwanted 2 μm laser emission. Second, for a too low Tm^{3+} doping level, the pump absorption efficiency will be significantly reduced. The Tm^{3+} doping level of 1.5 at.% could simultaneously provide sufficiently high pump absorption while keeping a relatively long $^3H_4$ level lifetime.

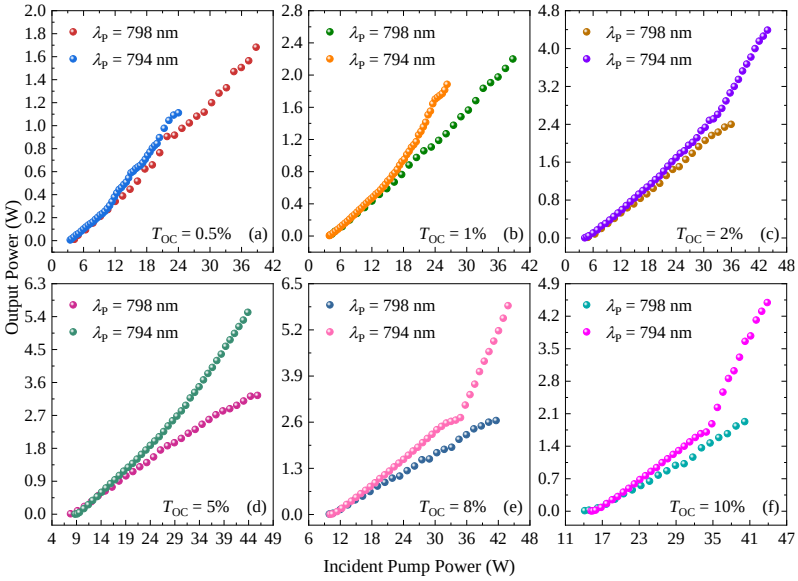

Fig. 5. Input-output dependences of the diode-pumped Tm:YVO_4 lasers at pumping at the strongest absorption (λ_P = 798 nm) and weaker absorption (λ_P = 794 nm): (a-f) 0.5%-10% OCs; λ_P - pump wavelength.

Pumped by the 798 nm laser diode, the power transfer characteristics were nearly linear, and no thermal rollover was observed for all the studied OCs in the Tm:YVO_4 laser. The maximum 2.3 μm CW laser output power of 3.25 W with a slope efficiency of 8.9% and a laser threshold of 7.79 W was obtained when using an intermediate output coupling of 5%. For other OCs, the corresponding maximum output powers were in the range of 2~3 Watts while the laser slope efficiencies were lower, about 8%.

Pumped by the 794 nm laser diode, for all the studied OCs, the slope efficiencies of the Tm:YVO_4 laser were higher than those in the case of 798-nm pumping. The highest CW laser output power of 5.52 W at 2.29 μm was obtained also for 5% OC. The corresponding slope efficiency increased gradually from 13% to 19.9% as the pump level increased. For smaller output coupling in the range of 0.5%-2%, there was a similar behavior of the gradual increase in the slope efficiency, with the values ranging from 3.9% to 6.1% for 0.5% OC, from 6.1% to 11.5% for 1% OC, and from 9.1% to 16.7% for 2% OC. We believe that it is mainly due to the positive action of the ETU effect, Tm_1 ($^3F_4$) + Tm_2 ($^3F_4$) → Tm_1 ($^3H_6$) + Tm_2 ($^3H_4$), which is a phonon-assisted process, being detrimental for the 1.9 μm laser transition but useful for the 2.3 μm one, see Fig. 1 (a). On increasing the pump power, the ground-state ($^3H_6$) is bleached and the Tm^{3+} ions accumulate in the metastable intermediate $^3F_4$ state, leading to the enhanced ETU probability, which is responsible for refilling the upper laser level ($^3H_4$) at the expense of the

$^3F_4$ population. Under these conditions, the pump quantum efficiency of the $^3H_4 \rightarrow {}^3H_5$ Tm^{3+} transition increases and may exceed unity representing a two-for-one pumping process [22].

The power transfer characteristics for high output coupling of 8%-10% were very different from those achieved for 0.5%-5% OCs. Indeed, they did not present a gradual increase in the slope efficiency but instead featured an abrupt and significant increase of this parameter at an incident pump power above 35.7 W, namely from 12% to 34% (8% OC) and from 10% to 28% (10% OC). The resulting maximum CW laser output power reached 5.88 W and 4.49 W, respectively. The laser emission spectra shown in Fig. 7 (b) demonstrate that at $P_{inc} > 35.7$ W, the Tm:YVO_4 laser simultaneously operated at 2.29 μm and 1.8 μm, which corresponded to the most intense emission peaks of the $^3H_4 \rightarrow {}^3H_5$ and $^3F_4 \rightarrow {}^3H_6$ Tm^{3+} transitions (for π-polarized light, cf. Fig. 2 (a)). Although both these OCs were coated for high transmission at ~2 μm to suppress oscillations on the $^3F_4 \rightarrow {}^3H_6$ transition, the Tm:YVO_4 laser still operated on a cascade scheme at higher pump levels. This is because of a significant accumulation of population in the metastable $^3F_4$ state at high pump levels and high output coupling rates enabling sufficient gain on the $^3F_4 \rightarrow {}^3H_6$ transition. The 2.29 μm power contribution was separated from the total output power (at 1.8 μm and 2.29 μm) by the long-pass filter F_2. The input-output dependences of the Tm:YVO_4 cascade laser are shown in Fig. 6 (a) and (b).

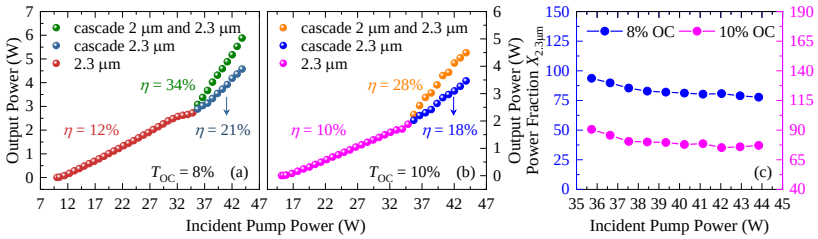

Fig. 6. Diode-pumped Tm:YVO_4 laser operating on the cascade scheme at 1.8 μm and 2.29 μm: (a,b) input-output dependences for different output coupling rates: (a) 8% OC and (b) 10% OC; (c) power fraction $X_{2.3μm}$ of the $^3H_4 \rightarrow {}^3H_5$ laser emission. λ_P = 794 nm.

Commented [ПП1]: The vertical scales in (c) should be the same!
Please do not exceed 100% in both cases, as it is confusing.

After filtering out the 1.8 μm power contribution, the maximum 2.29 μm CW laser output powers of 4.58 W and 3.46 W and slope efficiencies of 21% and 18% were obtained for 8% and 10% OCs, respectively. The ETU process is strongly reduced for the cascade laser due to the reduction of the $^3F_4$ state population down to the level established by the condition "gain is equal to losses". Consequently, we believe that the significant increase in the slope efficiency of the 2.3 μm laser for the cascade laser scheme as compared to operation solely on the $^3H_4 \rightarrow {}^3H_5$ transition, namely from 12% (no cascade laser) to 21% (cascade laser) for 8% OC and from 10% (no cascade laser) to 18% (cascade laser) for 10% OC, is due to the addition of the $^3F_4 \rightarrow {}^3H_6$ laser channel. It is mainly explained by the recycling of Tm^{3+} ions stored in the metastable intermediate $^3F_4$ state, which are forced down to the ground-state ($^3H_6$). The bottleneck effect leading to the ground-state bleaching is then efficiently avoided. The efficient high-power dual-waveband lasers simultaneously operating at 2 μm and 2.3 μm are promising for clinical medical treatment requiring realtime continuous non-invasive blood glucose monitoring, high-precision free-space telecommunications, and atmospheric environment monitoring supporting the detection of multiple gas components simultaneously.

Figure 6 (c) shows the power fraction ($X_{2.3μm} = P_{2.3μm}/P_\Sigma$) of the $^3H_4 \rightarrow {}^3H_5$ laser emission when colasing was allowed. Where $P_{2.3μm}$ and P_Σ are the 2.3 μm output power and the total output power, respectively. The power fraction $X_{2.3μm}$ decreased from 94% to 78% for 8% OC and from 91% to 77% for 10% OC with the pump level increased, indicating the presence of the gain competition between the $^3H_4 \rightarrow {}^3H_5$ and $^3F_4 \rightarrow {}^3H_6$ Tm^{3+} transition.

For 2%, 5%, and 8% OCs, all the obtained maximum ~2.3 μm CW laser powers reached a level of 4~6 Watts, surpassing the best results reported previously for other diode-pumped 2.3-

μm Tm lasers, namely 2.11 W for Tm:$LiYF_4$ [19], 1.49 W for Tm:YAG [35], and 2.97 W for Tm:$YAlO_3$ [38]. In the present work, the maximum CW output power of the 2.3-μm Tm-laser amounted to 5.52 W and further power scaling was limited by the available pump. Further power scaling of Tm:YVO_4 lasers is thus expected by employing more powerful laser diodes. In addition, the laser performance can be boosted by changing the pumping scheme to dual-end pumping or upconversion pumping, selecting a more suitable Tm^{3+} doping level, or by using composite laser crystals to mitigate thermal effects at high pump levels.

The laser emission spectra of the 794-nm laser diode-pumped Tm:YVO_4 laser captured just above the laser threshold and at the maximum applied pump power are shown in Fig. 7. Near the laser threshold, for low output coupling of 0.5%-2%, the Tm:YVO_4 laser operated only at 2.37 μm presenting a single laser line. For higher 5%-10% output coupling, the emission wavelength shifted to 2.29 μm presenting a single line in the spectrum. The two observed laser wavelengths of 2.29 μm and 2.37 μm correspond to the two most intense peaks in the stimulated-emission cross-section spectrum for the $^3H_4 \rightarrow {}^3H_5$ Tm^{3+} transition (for π-polarization), see Fig. 2 (a). At high pump levels, multiple longitudinal laser modes were observed. They are due to the etalon effect at the air gap between the PM and the Tm:YVO_4 crystal, as well as the relatively broad emission spectra of Tm^{3+} ions in YVO_4. For 1% and 2% OCs, the Tm:YVO_4 lasers operated in two spectral ranges, at 2.37 μm and 2.29 μm, with the power fraction of the former emission being dominant. Note that the 2.3 μm laser emission for all the laser configurations was linearly polarized (pure π-polarization).

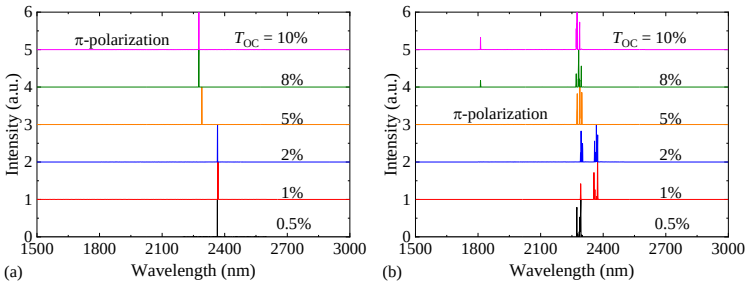

Fig. 7. Laser emission spectra from the 794-nm laser diode-pumped Tm:YVO_4 laser: (a) captured just above the laser threshold and (b) measured at the maximum applied pump power. The polarization of laser emission is π.

The beam quality was evaluated by both capturing the laser beam profile and measuring the M^2 parameters at a high pump level, as shown in Fig. 8 (a). The Tm:YVO_4 laser generated a nearly circular output beam. The measured M^2 parameters for the horizontal (X) and vertical (Y) directions were very close, M_x^2 = 1.49 and M_y^2 = 1.48, indicating laser operation on the fundamental transverse mode.

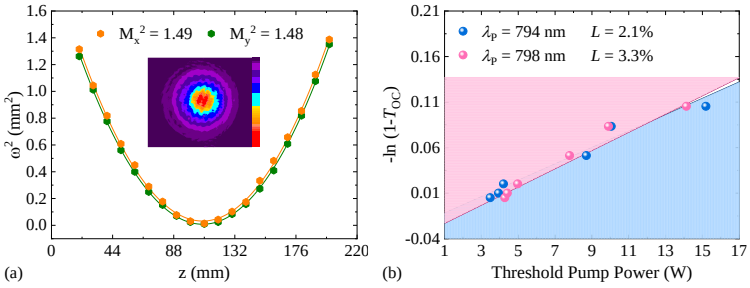

Fig. 8. (a) Evaluation of the beam quality parameters M^2 for the 794-nm laser diode-pumped Tm:YVO_4 laser with 5% OC, *inset*: 2D laser beam profile. (b) Findlay-Clay analysis for 794-nm and 798-nm pumped Tm:YVO_4 lasers, L - round-trip intracavity losses.

The round-trip resonator loss L in the diode-pumped quasi-four-level Tm:YVO_4 lasers was estimated using the Findlay-Clay analysis [39], as shown in Fig. 8 (b), yielding the L values of 2.1% and 3.3% for 794-nm and 798-nm pumping, respectively.

Table 2. Output Performance[a] of the Diode-Pumped ~2.3 μm 1.5 at.% Tm:YVO_4 CW Laser

λ_P (nm)	T_{OC} (%)	P_{th} (W)	P_{max} (W)	η (%)
794 (pumping at the weaker absorption)	0.5	3.48	1.11	3.90 to 6.10
	1	3.93	1.89	6.10 to 11.5
	2	4.20	**4.39**	9.10 to **16.7**
	5	8.70	**5.52**	13.0 to **19.9**
	8	10.1	**4.58**	11.8 to **21.3**
	10	15.2	**3.46**	9.60 to **17.7**
798 (pumping at the strongest absorption)	0.5	4.27	1.68	4.80
	1	4.41	2.20	6.30
	2	4.83	2.40	8.00
	5	7.79	**3.25**	**8.90**
	8	9.90	2.65	8.60
	10	14.1	1.93	7.60

[a] λ_P, pump wavelength; T_{OC}, transmission of the output coupler at ~2.3 μm; P_{th}, laser threshold power (incident pump power); P_{max}, maximum continuous wave laser output power; η, ~2.3 μm laser slope efficiency (vs. incident pump power). For 794-nm pumping, the slope efficiencies at low and high pump levels are given.

3.3 Passively Q-switched Tm:YVO_4 laser

The porous nano-grained cuprous selenide (PNG-Cu_2Se) has been demonstrated to have excellent mid-infrared nonlinear optical properties in our previous work [40], such as the large effective nonlinear absorption coefficient (20.0 cm·MW^{-1}), large modulation depth (11.9%), and low saturation intensity (131.4 kW·cm^{-2}) at ~2.3 μm. Passive Q-switching of the Tm:YVO_4 laser was investigated by using the 794 nm laser diode as a pump source. To reduce the insertion loss, the PNG-Cu_2Se alcohol solution was deposited directly on the 1% OC. As shown in Fig. 9 (a), the obtained maximum average output power was 0.23 W with a slope efficiency of 3.5%. Different from the CW Tm:YVO_4 laser with the same output coupling, the Q-switched laser

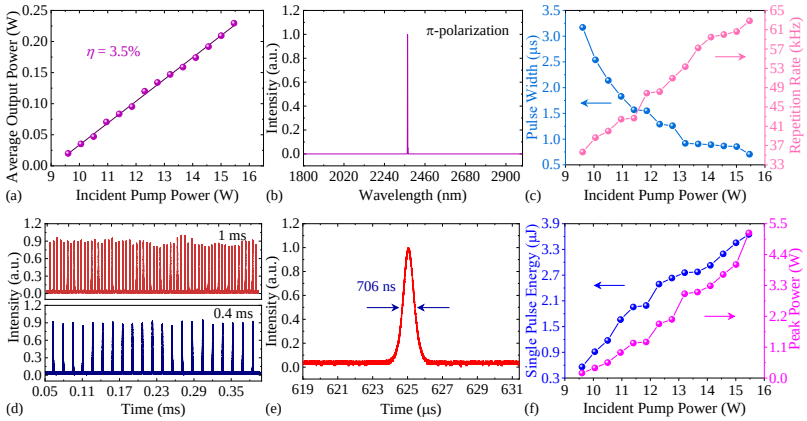

Fig. 9. Diode-pumped Tm:YVO_4 laser passively Q-switched by a PNG-Cu_2Se saturable absorber: (a) average output power, η - slope efficiency, (b) laser emission spectrum, (c) pulse

duration and pulse repetition rate, (d, e) oscilloscope traces of (d) a stable pulse train and (e) a single Q-switched pulse with the minimum pulse duration, and (f) single pulse energy and peak power. λ_P = 794 nm, T_{OC} = 1%.

operated only in one spectral range, at 2.37 μm (π-polarization), as shown in Fig. 9 (b). This spectrum was notably narrowed, which was related to the competition of longitudinal modes bleaching the saturable absorber resulting in a filtering of some of them. On increasing the pump level, the pulse duration monotonically decreased from 3.17 μs to 706 ns, and the corresponding pulse repetition rate increased from 35.66 kHz to 62.84 kHz, as shown in Fig. 9 (c). The stable pulse train in 1 ms and 0.4 ms time scales and the temporal profile of a single Q-switched pulse with the minimum pulse duration are shown in Fig. 9 (d) and (e), respectively. The peak-to-peak intensity fluctuations are estimated to be below 10% using the root-mean-square error method. According to the average output power and pulse repetition rate, the single pulse energy is calculated as 3.65 μJ, as shown in Fig.9 (f).

To the best of our knowledge, this is the first passively Q-switched Tm:YVO_4 laser operating on the $^3H_4 \rightarrow {}^3H_5$ transition.

4. Conclusion

To conclude, Tm^{3+}-doped yttrium orthovanadate crystals (Tm:YVO_4) are attractive for efficient diode-pumped 2.3-μm lasers power scalable to the multi-Watt level owing to a combination of good thermo-mechanical properties and appealing spectroscopic behavior for polarized light. By using a weaker absorption pumping scheme for alleviating thermal effects in high-power diode-pumped crystals, as well as the cascade laser strategy (simultaneous operation on the $^3H_4 \rightarrow {}^3H_5$ and $^3F_4 \rightarrow {}^3H_6$ Tm^{3+} transitions), the Tm:YVO_4 laser was scaled up to 5.52 W at 2.29 μm with a slope efficiency of 19.9% and a linear laser polarization (π). The selection of a moderate doping level (1.5 at.% Tm) was crucial for reaching these output characteristics.

Our work sheds light on the roles of energy-transfer upconversion from the intermediate metastable $^3F_4$ Tm^{3+} state, as well as cascade lasing involving a laser transition from this level ($^3F_4 \rightarrow {}^3H_6$) in boosting the 2.3-μm Tm laser performance. Two operation regimes are observed. Without colasing, a gradual increase in the slope efficiency of the 2.3 μm laser is assigned to the positive action of ETU refilling the upper laser level ($^3H_4$). When colasing is allowed, the laser slope efficiency at 2.3 μm rapidly changes as the $^3F_4 \rightarrow {}^3H_6$ laser drains the $^3F_4$ metastable state and prevents the bottleneck effect by reducing the ground-state bleaching. This effect has a major influence on the laser performance compared to that caused by ETU.

Finally, similarly to other rare-earth orthovanadates, Tm^{3+}-doped YVO_4 features very broad and nearly structureless gain profiles at 2.2 to 2.4 μm which suggests that this compound can potentially support the generation of ultrashort pulses from mode-locked lasers.

Funding. National Natural Science Foundation of China (12004213, 12174223, 12274263, 12304466, 52072351, 62175128). Qilu Young Scholar Program of Shandong University. Taishan Scholar Foundation of Shandong Province. French Agence Nationale de la Recherche (ANR) SPLENDID2 (ANR-19-CE08-0028), Normandy Region ("RELANCE" Chair of Excellence).

Disclosures. The authors declare no conflicts of interest.

Data availability. Data underlying the results presented in this paper are not publicly available at this time but may be obtained from the authors upon reasonable request.

References

1. S. Vasilyev, I. Moskalev, M. Mirov, V. Smolski, S. Mirov, and V. Gapontsev, "Ultrafast middle-IR lasers and amplifiers based on polycrystalline Cr:ZnS and Cr:ZnSe," Opt. Mater. Express **7**(7), 2636-2650 (2017).
2. N. Myoung, D. V. Martyshkin, V. V. Fedorov, and S. B. Mirov, "Energy scaling of 4.3 μm room temperature Fe:ZnSe laser," Opt. Lett. **36**(1), 94-96 (2011).
3. M. R. Majewski and S. D. Jackson, "Tunable dysprosium laser," Opt. Lett. **41**(19), 4496-4498 (2016).
4. P. A. Budni, M. L. Lemons, J. R. Mosto, and E. P. Chicklis, "High-power/high-brightness diode pumped 1.9-μm Thulium and resonantly pumped 2.1-μm Holmium lasers," IEEE J. Sel. Top. Quantum Electron. **6**(4), 629-635 (2000).

5. H. Uehara, R. Yasuhara, S. Tokita, J. Kawanaka, M. Murakami, and S. Shimizu, "Efficient continuous wave and quasi-continuous wave operation of a 2.8 μm Er:Lu_2O_3 ceramic laser," Opt. Express **25**(16), 18677-18684 (2017).
6. P. Camy, J.-L. Doualan, S. Renard, A. Braud, V. Ménard, and R. Moncorgé, "Tm^{3+}:CaF_2 for 1.9 μm laser operation," Opt. Commun. **236**(4-6), 395-402 (2004).
7. J. T. Olesberg, M. A. Arnold, C. Mermelstein, J. Schmitz, and J. Wagner, "Tunable laser diode system for noninvasive blood glucose measurements," Appl. Spectrosc. **59**(12), 1480-1484 (2005).
8. X. Chao, J. B. Jeffries, and R. K. Hanson, "Real-time, in situ, continuous monitoring of CO in a pulverized-coal-fired power plant with a 2.3 μm laser absorption sensor," Appl. Phys. B **110**(3), 359-365 (2013).
9. V. Petrov, "Frequency down-conversion of solid-state laser sources to the mid-infrared spectral range using non-oxide nonlinear crystals," Prog. Quantum Electron. **42**, 1-106 (2015).
10. Y. Sato and T. Taira, "The studies of thermal conductivity in $GdVO_4$, YVO_4, and $Y_3Al_5O_{12}$ measured by quasi-one-dimensional flash method," Opt. Express **14**(22), 10528-10536 (2006).
11. J. Šulc, P. Koranda, P. Černý, H. Jelínková, Y. Urata, M. Higuchi, W. Ryba-Romanowski, R. Lisiecki, P. Solarz, G. Dominiak-Dzik, and M. Sobczyk, "Tunable lasers based on diode pumped Tm-doped vanadates Tm:YVO_4, Tm:$GdVO_4$, and Tm:$LuVO_4$," Proc. SPIE **6871**, 68711V (2008).
12. P. Loiko, J. Bogusławski, J. M. Serres, E. Kifle, M. Kowalczyk, X. Mateos, J. Sotor, R. Zybała, K. Mars, A. Mikuła, K. Kaszyca, M. Aguiló, F. Díaz, U. Griebner, and V. Petrov, "Sb_2Te_3 thin film for the passive Q-switching of a Tm:$GdVO_4$ laser," Opt. Mater. Express **8**(7), 1723-1732 (2018).
13. C. P. Wyss, W. Lüthy, H. P. Weber, V. I. Vlasov, Y. D. Zavartsev, P. A. Studenikin, A. I. Zagumennyi, and I. Shcherbakov, "Performance of a Tm^{3+}:$GdVO_4$ microchip laser at 1.9 μm," Opt. Commun. **153**(1-3), 63-67 (1998).
14. K. Ohta, H. Saito, M. Obara, and N. Djeu, "Characterization of a longitudinally pumped CW, room-temperature operation of Tm^{3+}:YVO_4 laser," Jpn. J. Appl. Phys. **32**(4), 1651-1657 (1993).
15. X. Yu, H. Chu, F. Zha, H. Pan, S. Zhao, Z. Pan, and D. Li, "Watt-level diode-pumped Tm:YVO_4 laser at 2.3 μm," Opt. Lett. **47**(21), 5501-5504 (2022).
16. X. Yu, Z. Pan, H. Chu, F. Zha, H. Pan, L. Ma, P. Loiko, P. Camy, and D. Li, "Cascade lasing at ~2 μm and ~2.3 μm in a diode-pumped Tm:YVO_4 laser," Opt. Express **31**(9), 13576-13584 (2023).
17. X. Yu, Z. Pan, H. Chu, H. Pan, S. Zhao, and D. Li, "Diode-pumped efficient high-power cascade Tm:$GdVO_4$ laser simultaneously operating at ~2 μm and ~2.3 μm," Opt. Express **31**(16), 26368-26377 (2023).
18. X. Yu, K. Eremeev, Z. Pan, P. Loiko, H. Chu, H. Pan, S. Zhao, A. Braud, P. Camy, and D. Li, "Six-watt diode-pumped Tm:$GdVO_4$ laser at 2.29 μm," Opt. Lett. **48**(24), 6404-6407 (2023).
19. E. Kifle, P. Loiko, L. Guillemot, J.-L. Doualan, F. Starecki, A. Braud, T. Georges, J. Rouvillain, and P. Camy, "Watt-level diode-pumped thulium lasers around 2.3 μm," Appl. Optics **59**(25), 7530-7539 (2020).
20. L. Guillemot, P. Loiko, E. Kifle, J.-L. Doualan, A. Braud, F. Starecki, T. Georges, J. Rouvillain, A. Hideur, and P. Camy, "Watt-level mid-infrared continuous-wave Tm:YAG laser operating on the $^3H_4 \rightarrow {}^3H_5$ transition," Opt. Mater. **101**, 109745 (2020).
21. L. Guillemot, P. Loiko, A. Braud, J.-L. Doualan, A. Hideur, M. Koselja, R. Moncorge, and P. Camy, "Continuous-wave Tm:$YAlO_3$ laser at ~2.3 μm," Opt. Lett. **44**(20), 5077-5080 (2019).
22. P. Loiko, R. Soulard, L. Guillemot, G. Brasse, J.-L. Doualan, A. Braud, A. Tyazhev, A. Hideur, F. Druon, and P. Camy, "Efficient Tm:$LiYF_4$ lasers at ~2.3 μm: effect of energy-transfer upconversion," IEEE J. Quantum Electron. **55**(6), 1700212 (2019).
23. S. Tessarin, M. Lynch, J. F. Donegan, and G. Mazé, "Tm^{3+}-doped ZBLAN fibre amplifier at 1.49 μm with co-operative lasing at 1.88 μm," Electron. Lett. **41**(16), 899-900 (2005).
24. B. Schmaul, G. Huber, R. Clausen, B. Chai, P. LiKamWa, and M. Bass, "Er^{3+}:$YLiF_4$ continuous wave cascade laser operation at 1620 and 2810 nm at room temperature," Appl. Phys. Lett. **62**(6), 541-543 (1993).
25. L. Esterowitz, R. C. Eckardt, and R. E. Allen, "Long-wavelength stimulated emission via cascade laser action in Ho:YLF," Appl. Phys. Lett. **35**(3), 236-239 (1979).
26. S. Ye, X. Zhou, S. Huang, H. Nie, J. Bian, T. Li, K. Yang, J. He, and B. Zhang, "Cascade MIR Ho:YLF laser at 2.1 μm and 2.9 μm," Opt. Lett. **47**(21), 5642-5645 (2022).
27. S. Sujecki, L. Sójka, E. Bereś-Pawlik, Z. Tang, D. Furniss, A. B. Seddon, and T. M. Benson, "Modelling of a simple Dy^{3+} doped chalcogenide glass fibre laser for mid-infrared light generation," Opt. Quantum Electron. **42**(2), 69-79 (2010).
28. H. Dupont, P. Loiko, A. Tyazhev, L. Giordano, Z. Pan, H. Chu, D. Li, B. Viana, A. Hideur, L. Guillemot, A. Braud, P. Camy, P. Georges, and F. Druon, "Tm:CALGO lasers at 2.32 μm: cascade lasing and upconversion pumping," Opt. Express **31**(12), 18751-18764 (2023).
29. H. Dupont, L. Guillemot, P. Loiko, R. M. Solé, X. Mateos, M. Aguiló, F. Díaz, A. Braud, P. Camy, P. Georges, and F. Druon, "Cascade laser optimization for $^3H_4 \rightarrow {}^3H_5$ and $^3F_4 \rightarrow {}^3H_6$ sequent transitions in Tm^{3+}-doped materials," Opt. Express **31**(21), 34201-34212 (2023).
30. Q. Ma, H. Mo, and J. Zhao, "High-energy high-efficiency Nd:YLF laser end-pump by 808 nm diode," Opt. Commun. **413**, 220-223 (2018).
31. Y. Li, W. Chen, H. Lin, D. Ke, G. Zhang, S. Zhu, and Z. Chen, "Comparative investigation of diode-wing-pumped Tm:$Y_3Al_5O_{12}$ laser between composite and non-composite crystal," Opt. Laser Technol. **63**, 132-136, 2014.
32. X. Yu, K. Eremeev, Z. Pan, P. Loiko, H. Chu, H. Pan, A. Braud, P. Camy, and D. Li, "Crystal growth, polarized spectral properties, and 2.3 μm laser performance of Tm:$LuVO_4$ crystal," submitted to Optics Express.

33. I. Razumova, A. Tkachuk, A. Nikitichev, and D. Mironov, "Spectral-luminescent properties of Tm:YLF crystal," J. Alloy. Compd. **225**(1-2), 129-132 (1995).
34. L. Guillemot, P. Loiko, R. Soulard, A. Braud, J.-L. Doualan, A. Hideur, and P. Camy, "Close look on cubic Tm:KY_3F_{10} crystal for highly efficient lasing on the $^3H_4 \rightarrow {}^3H_5$ transition," Opt. Express **28**(3), 3451-3463 (2020).
35. F. Zha, X. Yu, H. Chu, H. Pan, S. Zhao, P. Loiko, Z. Pan, and D. Li, "Compact diode-pumped continuous wave and passively Q switched Tm:YAG laser at 2.33 μm," Opt. Lett. **47**(23), 6265-6268 (2022).
36. B. F. Aull, and H. P. Jenssen, "Vibronic interactions in Nd:YAG resulting in nonreciprocity of absorption and stimulated emission cross sections," IEEE J. Quant. Electron. **18**(5), 925-930 (1982).
37. R. Lisiecki, P. Solarz, G. Dominiak-Dzik, W. Ryba-Romanowski, M. Sobczyk, P. Černý, J. Šulc, H. Jelínková, Y. Urata, and M. Higuchi, "Comparative optical study of thulium-doped YVO_4, $GdVO_4$, and $LuVO_4$ single crystals," Phys. Rev. B **74**(3), 035103 (2006).
38. X. Yu, F. Zha, Z. Pan, H. Chu, H. Pan, and D. Li, "Diode-pumped Tm:YAP laser operating at 2.3 μm with enhanced performance through cascade lasing," Opt. Express **32**(3), 3461-3469 (2024).
39. J. A. Caird, S. A. Payne, P. R. Staver, A. J. Ramponi, L. L. Chase, and W. F. Krupke, "Quantum electronic properties of the $Na_3Ga_2Li_3F_{12}:Cr^{3+}$ laser," IEEE J. Quantum Electron. **24**(6), 1077-1099 (1988).
40. X. Yu, H. Yuan, Z. Pan, H. Pan, H. Chu, and D. Li, "Porous nano-grained cuprous selenide (Cu_2Se) for mid-infrared photonics," J. Alloy. Compd. **987**, 174179 (2024).